

Title page

Difference in Mechanism-Based Inhibition of Cytochrome P450 3A4 and 3A5 by a
Series of Fluoroquinolone Antibacterial Agents

Akiko Watanabe, Hideo Takakusa, Takako Kimura, Shin-ichi Inoue, Hiroyuki
Kusuhara, and Osamu Ando

Drug Metabolism and Pharmacokinetics Research Laboratories, Daiichi Sankyo Co.,
Ltd., Tokyo, Japan (A.W., H.T., S.I., O.A.)

Structural Biology Group, Biological Research Department, Daiichi Sankyo RD Novare
Co., Ltd., Tokyo, Japan (T.K.)

Laboratory of Molecular Pharmacokinetics, Graduate School of Pharmaceutical
Sciences, The University of Tokyo, Japan (H.K.)

Running title page

Running title: Mechanism-Based Inhibition of CYP3A5 by Fluoroquinolones

Address Correspondence to:

Akiko Watanabe

1-2-58, Hiromachi, Shinagawa-ku, Tokyo 140-8710, Japan

Telephone: +81 3-3492-3131

Fax: +81 3-5436-8567

E-mail: watanabe.akiko.mi@daiichisankyo.co.jp

Number of Text Pages: 17

Number of Tables: 2

Number of Figures: 6

Number of References: 20

Number of Words in Abstract: 204

Number of Words in Introduction: 563

Number of Words in Discussion: 825

List of nonstandard abbreviations

MBI, mechanism-based inhibition

CYP, cytochrome P450

MI, metabolite-intermediate complex

HLM, human liver microsome

LC, liquid chromatography

MS, mass spectrometry

PDB, Protein Data Bank

Abstract

A series of fluoroquinolone antibacterial compounds were found to be irreversible (compounds 1–5) and quasi-irreversible (compounds 6–9) inhibitors of cytochrome P450 3A4 (CYP3A4). The purpose of this study was to evaluate their mechanism-based inhibition (MBI) potency against CYP3A5. Compounds 1–5 were also irreversible inhibitors of CYP3A5, whereas compounds 6–9 showed neither irreversible nor quasi-irreversible inhibition of CYP3A5. Compounds 6 and 8 did not form a metabolite-intermediate (MI) complex with the heme of CYP3A5 during incubation. The structural analysis of the metabolites after incubation of compounds 1 and 6 with CYP3A5 revealed that their metabolites were identical to those produced by CYP3A4, including the precursors of which are speculated to account for the MBI of CYP3A4. The homology modeling of CYP3A5 suggests that four residues around the nitroso intermediate of compound 6 in the substrate-binding pocket of CYP3A4 correspond with the bulkier residues in CYP3A5, especially, Phe210 in CYP3A5, which might contribute to the steric hindrance with the nitroso intermediate of compound 6. The substrate-binding pocket structure of CYP3A5 might prevent the nitroso intermediate from coordinate binding with the heme, thereby preventing quasi-irreversible inhibition.

Our study may provide new insights into the observable differences between the inhibition of CYP3A4 and CYP3A5.

Introduction

Cytochrome P450 (CYP) 3A is an important member of the P450 subfamily. CYP3A4 and CYP3A5 are the major isoforms of CYP3A because they are responsible for the metabolism of more than 50% of marketed drugs (Thummel and Wilkinson, 1998; Wilkinson, 2005). CYP3A4 and CYP3A5 show an 83% homology in their amino acid sequences; therefore, the substrate specificity of these isoforms overlaps (de Wildt et al., 1999; Niwa et al., 2014). CYP3A5 is polymorphically expressed in the human liver and intestine, and thereby, causes inter-individual variations in the disposition of CYP3A substrates such as midazolam and nifedipine (Lamba et al., 2002).

Despite the highly conserved amino acid residues of both isoforms, the effect of some of their inhibitors, especially time-dependent inhibitors, apparently differs between CYP3A4 and CYP3A5. Generally, the inhibitors showed a weaker effect on CYP3A5 than they did on CYP3A4 (Niwa et al., 2008). Raloxifene irreversibly inhibited CYP3A4, but not CYP3A5 (Pearson et al., 2007). The reactive intermediate binds covalently to an apoprotein of CYP3A4, and the difference in the amino acid residue modified by the reactive intermediate between the two isoforms (cysteine and serine at position 239 for CYP3A4 and CYP3A5, respectively) could account for the difference in susceptibility. Erythromycin, diltiazem, nifedipine, verapamil, and lapatinib showed

quasi-irreversible inhibition of CYP3A4, in which the metabolite intermediates form stable complexes with the heme (MI complex). However, such complexes were not observed with CYP3A5 (McConn et al., 2004; Wang et al., 2005; Takakusa et al., 2011).

In the case of lapatinib, the difference in the susceptibility was attributable to their ability to generate the hydroxylamine metabolite (M3), which was followed by the generation of a nitroso intermediate forming the MI complex with the heme. However, CYP3A5 generates other metabolites (M1 and M4) at a similar or slightly lower level than CYP3A4 does (Takakusa et al., 2011). In addition to the ability to generate the metabolite intermediate, it is possible that the structure of the substrate-binding pocket of CYP3A5 limits the intermediates' access to the heme or disturbs the formation of the appropriate configuration of the reactive intermediate required to interact with the heme.

Previously, we established an assay to distinguish between irreversible and quasi-irreversible inhibition based on the mechanism involving the dissociation of MI complexes after treatment with potassium ferricyanide, which oxidizes the heme iron to the ferric form and recovers the enzymatic activity (Buening and Franklin, 1976; Muakkassah et al., 1982; Watanabe et al., 2007). Using this MBI reversibility assay, we demonstrated that a series of fluoroquinolone antibacterial compounds (compounds 1–9) are irreversible or quasi-reversible inhibitors (compounds 1–5 and 6–9,

respectively) that contain either cyclopropylamine in the pyrrolidine ring or an amine moiety in the ring form of the 7'-position of fluoroquinolone, respectively. The difference in the ring structure bearing a primary amine group in quinolones may determine their MBI mechanisms. In addition, compound 10, formed by the introduction of a methyl group at the carbon atom at the root of the C7-amino moiety of compound 8, did not inhibit CYP3A4 despite its production of a nitroso intermediate, presumably owing to the steric hindrance of the methyl moiety (Watanabe et al., 2016). In this study, we investigated the irreversible or quasi-irreversible inhibition of CYP3A5 by the fluoroquinolone derivatives. We report here that while irreversible inhibition was common for CYP3A4 and CYP3A5, quasi-reversible inhibition was not, although CYP3A5 also produced nitroso intermediates.

Materials and Methods

Materials. All the tested fluoroquinolone compounds shown in Table 1 were synthesized by Daiichi Sankyo Co., Ltd. (Tokyo, Japan). The synthesis method of compound 10 as a representative fluoroquinolone compound was described in a previous report (Odagiri et al., 2013). Midazolam maleate salt was purchased from Sigma-Aldrich (St. Louis, MO, USA). 1'-Hydroxymidazolam was purchased from Ultrafine (Manchester, UK). Potassium phosphate buffer (0.5 M), [$^{13}\text{C}_3$]hydroxymidazolam, NADPH Regenerating System Solution A and B, and recombinant human CYP3A5 Supersomes containing P450 reductase and cytochrome b5 were acquired from Corning (Woburn, MA). Potassium ferricyanide was purchased from Kanto Chemical Co. Inc. (Tokyo, Japan). All other reagents and solvents were of the highest grade commercially available.

Reversibility of MBI using Recombinant Human CYP3A5 Supersomes. This assay was performed as described previously (Watanabe et al., 2016). Briefly, recombinant human CYP3A5 Supersomes (final concentration 10 pmol/mL) were preincubated with test compound (final concentration 30 or 100 μM) for 0 or 30 minutes, the preincubation solution was mixed with or without potassium ferricyanide (final concentration 1 mM), and then this was incubated for 10 minutes. The metabolic

activity of the incubation solution was determined by incubating it with 25 μ M midazolam as a substrate for 10 minutes and then monitoring the concentration of 1'-hydroxymidazolam by liquid chromatography (LC)–tandem mass spectrometry (MS/MS) using a system that consisted of a Waters Acquity UPLC and TQD (Waters, Manchester, UK). The percentage of metabolic activity [% of control_(0 minutes) and % of control_(30 minutes)] and the percentage of the enzymatic activity remaining (% remaining) after 30-minute preincubation relative to 0-minute preincubation were calculated as follows and are detailed in previous reports (Watanabe et al., 2007; Watanabe et al., 2016).

$$\% \text{ of control}_{(0 \text{ minutes})} = \frac{v_{(0 \text{ minutes}, + \text{inhibitor})}}{v_{(0 \text{ minutes}, - \text{inhibitor})}} \times 100$$

$$\% \text{ of control}_{(30 \text{ minutes})} = \frac{v_{(30 \text{ minutes}, + \text{inhibitor})}}{v_{(30 \text{ minutes}, - \text{inhibitor})}} \times 100$$

$$\% \text{ remaining} = \frac{\% \text{ of control}_{(30 \text{ minutes})}}{\% \text{ of control}_{(0 \text{ minutes})}} \times 100$$

where, $v_{(0 \text{ minutes}, \pm \text{inhibitor})}$ is the metabolic activity after 0-minute preincubation with (+) or without an inhibitor, and $v_{(30 \text{ minutes}, \pm \text{inhibitor})}$ is the metabolic activity after 30-minute preincubation with (+) or without an inhibitor.

Absorption Analysis for MI Complex Formation. The NADPH-generating system was added to the reaction mixture containing 100 pmol/mL recombinant human CYP3A5 Supersomes with test compounds (final concentration 50 μ M), and then the absorbance was monitored at 455 and 490 nm for 20 minutes as described previously (Watanabe et al., 2016).

Structural Elucidation of Metabolites of Test Compounds after Incubation with Recombinant Human CYP3A5 Supersomes. The reaction mixture was incubated with recombinant human CYP3A5 Supersomes (final concentration 100 pmol/mL) in the presence of test compounds (final concentration 50 μ M) for 30 minutes, and then analyzed by LC-MS/MS using an LTQ-Orbitrap XL (Thermo Fisher Scientific, San Jose, CA) equipped with an Acquity UPLC PDA system (Waters) as described previously (Watanabe et al., 2016).

CYP3A5 Homology Modeling. The homology modeling of CYP3A5 was performed using the Prime homology modeling module of Maestro (version 4.1, Schrödinger, LLC) based on the crystal structure of CYP3A4 (PDB code 4I4G) (Sevrioukova and Poulos, 2013). Starting with the amino acid sequence of CYP3A5 (UniProt code P20815) that was aligned with the sequence of CYP3A4, the initial CYP3A5 model was constructed by copying the coordinate of the CYP3A4 crystal structure with the

mutation to the CYP3A5 amino acid in a different amino-acid position. The side chains of the mutation site of the initial CYP3A5 model were refined using the Prime protein refinement module of Maestro.

Results

Reversibility of MBI of CYP3A5 by Fluoroquinolones. To investigate the inhibition of CYP3A5 by a series of irreversible and quasi-irreversible inhibitors (compounds 1–5 and 6–9, respectively), and the noninhibitor or weak inhibitor, compound 10, of CYP3A4 (Watanabe et al., 2016), the MBI reversibility assay was performed in recombinant human CYP3A5 Supersomes (Fig. 1). The enzymatic activity of CYP3A5 monitored as the activity of 1'-hydroxymidazolam formation from midazolam was inactivated after 30-minute preincubation with each compound (1–5), and the reduced enzymatic activity was not restored by incubation with potassium ferricyanide. This result indicates that compounds 1–5 inactivated CYP3A5 irreversibly. The inhibitory potential of CYP3A4 and CYP3A5 by these compounds was compared (Table 2). For compounds 1–5, the % remaining value after 30-minute preincubation with CYP3A5 was almost comparable with or slightly higher than that with CYP3A4. In contrast, the enzymatic activity of CYP3A5 was unchanged even after 30-minute preincubation with compounds 6–10 at least at the concentrations tested.

Absorption Analysis for MI Complex Formation. The formation of an MI complex with the heme of CYP3A5 was confirmed by monitoring the absorbance difference between 455 and 490 nm for 20 minutes after the addition of the NADPH-generating

system in the reaction mixture containing recombinant CYP3A5 Supersomes and each test compound (Fig. 2). The absorbance difference was not changed during the incubation period for compounds 6, 8, and 10. This observation suggests that compounds 6, 8, and 10 did not form an MI complex with the heme of CYP3A5.

Structural Elucidation of Metabolites of Compounds 1 and 6 after Incubation with Recombinant CYP3A5 Supersomes. To compare the metabolic profiles of the fluoroquinolone compounds between CYP3A4 and CYP3A5, we carried out a structural analysis by LC-MS/MS of the metabolites after incubating CYP3A5 with compound 1, a representative irreversible inhibitor of both CYP3A4 and CYP3A5. The analysis showed four metabolites related to oxidation reactions of the cyclopropylamine moiety of compound 1 (Supplemental Fig. 1). The proposed structure of each metabolite is shown in Fig. 3. All the metabolites of compound 1 detected after incubation with CYP3A5 were also detected following incubation with CYP3A4 (Watanabe et al., 2016). In addition, we performed a structural analysis of metabolites after incubating CYP3A5 with compound 6, a representative quasi-irreversible inhibitor of CYP3A4 but not CYP3A5. The analysis revealed five metabolites related to oxidation reactions of the amino azaspiro[4.4]nonan moiety of compound 6 (Supplemental Fig. 2). The proposed structure of each metabolite is shown in Fig. 4. The metabolites of compound

6 detected following its metabolism by CYP3A5 were unexpectedly identical to those generated by CYP3A4 (Watanabe et al., 2016).

CYP3A5 Homology Modeling. To study the substrate-binding pocket of CYP3A5, the homology model of CYP3A5 was constructed for amino acid residues 27-495, which corresponded to the CYP3A4 crystal structure (Fig. 5A). The homology model of CYP3A5 was superposed by the docking model of compound 6 and its nitroso metabolite to CYP3A4 obtained in the previous study (Watanabe et al., 2016) (Fig. 5B and C, respectively). The model suggests that nine hydrophobic residues (Phe57, Gln79, Phe108, Ile120, Leu210, Thr224, Val240, Ile369, and Met371) around the nitroso intermediate of compound 6 in the substrate-binding pocket of CYP3A4 are different in CYP3A5, which has the following corresponding residues: Leu57, Leu79, Leu108, Leu120, Phe210, Ile224, Leu240, Val369, and Ile371. Among the different amino acid residues, four (Leu108, Leu120, Phe210, and Leu240) in CYP3A5 were bulkier than the corresponding residues in CYP3A4. Furthermore, we also speculated that the Phe210 in CYP3A5 might cause steric hindrance with the nitroso intermediate, but not with compound 6. Regarding the difference in the MI complex formation of the nitroso intermediate of compound 6 between CYP3A4 and CYP3A5, we focused on the amino acid residues at position 210 of CYP3A4 and CYP3A5. Interestingly, as shown in Fig. 6,

the distance between the side chain of Phe210 in CYP3A5 and the closest side chain of the nitroso intermediate was 1.35 Å, while the distance between the side chain of Leu210 in CYP3A4 and the closest side chain of the nitroso intermediate was 4.63 Å. Therefore, there would be a steric clash between Phe210 in CYP3A5 and the nitroso intermediate.

Discussion

In this study, we focused on the difference in the inhibition of CYP3A4 and CYP3A5 by a series of fluoroquinolone antibacterial compounds, which are irreversible and quasi-irreversible inhibitors (compounds 1–5 and 6–9, respectively) of CYP3A4 (Watanabe et al., 2016). We investigated the inhibition of CYP3A5 by these fluoroquinolones by evaluating their MBI reversibility using recombinant human CYP3A5 Supersomes (Fig. 1) and compared the inhibitory potential between CYP3A4 and CYP3A5 (Table 2). Compounds 1–5 irreversibly inhibited CYP3A5 with similar (compound 1, 2, and 4) or somewhat lower potency (compound 3 and 5) than that on CYP3A4 (Table 2). In contrast, compounds 6–10 showed no inhibition of CYP3A5 at the concentration examined (Fig. 1 and Table 2); however, compounds 6–9 sufficiently inhibited CYP3A4 at the same or lower concentration. As reported for other CYP3A4 quasi-irreversible inhibitors (McConn et al., 2004; Wang et al., 2005; Niwa et al., 2008; Takakusa et al., 2011), the effects on CYP3A5 were clearly different from those on CYP3A4. Consistent with the lack of quasi-irreversible inhibition, compounds 6, 8, and 10 did not form an MI complex with the heme of CYP3A5 (Fig. 2).

The metabolites generated after incubating the fluoroquinolones with recombinant human CYP3A5 Supersomes were structurally analyzed to compare their profiles with

those of the metabolites produced by CYP3A4. All the metabolites of compound 1 detected following incubation with CYP3A4 (Watanabe et al., 2016) were detected after incubation with CYP3A5 Supersomes (Fig. 3). We speculated that cpd1-M3 was formed via the radical intermediate that covalently binds to CYP3A4 (Watanabe et al., 2016). The generation of cpd1-M3 by CYP3A5 suggests that the same mechanism underlies the irreversible inhibition of CYP3A5 by compound 1.

In addition, the metabolites of compound 6 detected following its metabolism by CYP3A5 were also unexpectedly identical to those generated by CYP3A4 (Watanabe et al., 2016) (Fig. 4). Importantly, the metabolites include cpd6-M3, the oxime form, which was supposed to be generated via the nitroso intermediate (Mansuy et al., 1977). Therefore, CYP3A5 generates the nitroso intermediate although the intermediate no longer forms an MI complex with the heme of CYP3A5 (Fig. 2). The peak area of the metabolite in the mass chromatogram of CYP3A5 was comparable to that of CYP3A4 (data not shown); however, further quantitative investigations would be required to conclude that the activities of CYP3A4 and CYP3A5 were similar in generating this intermediate.

To form a stable MI complex, the nitroso group must maintain an appropriate distance and angle from the core of the heme (C-N-Fe) (Negre et al., 2006). The

substrate-binding pocket of CYP3A5 may prevent the MI complex formation with the nitroso intermediate of our fluoroquinolones. To test this hypothesis, we constructed the homology model of CYP3A5 (Fig. 5A), which was superposed by the docking model of compound 6 and its nitroso metabolite to CYP3A4 obtained in the previous study (Watanabe et al., 2016) (Fig. 5B and C, respectively). The model indicated that the amino acid residues around the nitroso intermediate of compound 6 in the substrate-binding pocket of CYP3A5 were bulkier than the corresponding residues in CYP3A4. This observation is consistent with the results indicating that the CYP3A4 pharmacophore generated based on the in vitro data of the inhibitors is larger than that of CYP3A5 and 3A7 (Ekins et al., 2003). Among these bulky amino acid residues, Phe210 in CYP3A5 might cause steric hindrance with the nitroso intermediate, but not with compound 6 (Fig. 6). The 210-amino acid residue of CYP3A4 and CYP3A5 could also be important for recognizing aflatoxin B1 (Wang et al., 1998). A mutation involving the replacement of Leu with Phe at residue 210 in CYP3A4 revealed that its regioselectivity in aflatoxin B1 metabolism was similar to that of CYP3A5.

This study highlighted the difference in the susceptibility of CYP3A4 and CYP3A5 to quasi-irreversible inhibition by compounds 6–9 despite the generation of metabolites that could potentially form the MI complex with the heme. Furthermore, it also

demonstrated that in contrast, the susceptibility of the isoforms to irreversible inhibition by compounds 1–5 was similar. In addition to the ability to generate the nitroso intermediate, we speculate that the difference in the substrate-binding pocket also contributes to the differential susceptibility of the isoforms. Compound 10 did not show quasi-irreversible inhibition of CYP3A5 as was observed for CYP3A4, which was possibly owing to the steric hindrance of the methyl group with the heme (Watanabe et al., 2016). In addition to designing compounds to prevent the production of the nitroso intermediate, the introduction of a moiety to inhibit MI complex formation would be another key strategy to avoid MBI in future drug development processes.

In conclusion, we demonstrated that the fluoroquinolone antibacterial compounds 1–5 irreversibly inhibited both CYP3A4 and CYP3A5, whereas compounds 6–9 showed quasi-irreversible inhibition of CYP3A4 but not CYP3A5. Our study may provide new insights into the differential effects of the tested compounds as evidenced by the quasi-irreversible inhibition of CYP3A4 but not CYP3A5.

Authorship Contributions.

Participated in research design: Watanabe, Kusuhara

Conducted experiments: Watanabe, Takakusa, Kimura

Contributed new reagents or analytical tools: Watanabe, Takakusa, Kimura

Performed data analysis: Watanabe, Takakusa, Kimura

Wrote or contributed to the writing of the manuscript: Watanabe, Takakusa, Kimura,

Inoue, Kusuhara, Ando

References.

- Buening MK and Franklin MR (1976) SKF 525-A inhibition, induction, and 452-nm complex formation. *Drug Metab Dispos* **4**:244-255.
- de Wildt SN, Kearns GL, Leeder JS, and van den Anker JN (1999) Cytochrome P450 3A: ontogeny and drug disposition. *Clin Pharmacokinet* **37**:485-505.
- Ekins S, Stresser DM, and Williams JA (2003) In vitro and pharmacophore insights into CYP3A enzymes. *Trends Pharmacol Sci* **24**:161-166.
- Lamba JK, Lin YS, Schuetz EG, and Thummel KE (2002) Genetic contribution to variable human CYP3A-mediated metabolism. *Advanced drug delivery reviews* **54**:1271-1294.
- Mansuy D, Gans P, Chottard JC, and Bartoli JF (1977) Nitrosoalkanes as Fe(II) ligands in the 455-nm-absorbing cytochrome P-450 complexes formed from nitroalkanes in reducing conditions. *Eur J Biochem* **76**:607-615.
- McConn DJ, 2nd, Lin YS, Allen K, Kunze KL, and Thummel KE (2004) Differences in the inhibition of cytochromes P450 3A4 and 3A5 by metabolite-inhibitor complex-forming drugs. *Drug Metab Dispos* **32**:1083-1091.

- Muakkassah SF, Bidlack WR, and Yang WC (1982) Reversal of the effects of isoniazid on hepatic cytochrome P-450 by potassium ferricyanide. *Biochem Pharmacol* **31**:249-251.
- Negrerie M, Kruglik SG, Lambry JC, Vos MH, Martin JL, and Franzen S (2006) Role of heme iron coordination and protein structure in the dynamics and geminate rebinding of nitric oxide to the H93G myoglobin mutant: implications for nitric oxide sensors. *J Biol Chem* **281**:10389-10398.
- Niwa T, Murayama N, Emoto C, and Yamazaki H (2008) Comparison of kinetic parameters for drug oxidation rates and substrate inhibition potential mediated by cytochrome P450 3A4 and 3A5. *Current drug metabolism* **9**:20-33.
- Niwa T, Yasumura M, Murayama N, and Yamazaki H (2014) Comparison of catalytic properties of cytochromes P450 3A4 and 3A5 by molecular docking simulation. *Drug metabolism letters* **8**:43-50.
- Odagiri T, Inagaki H, Sugimoto Y, Nagamochi M, Miyauchi RN, Kuroyanagi J, Kitamura T, Komoriya S, and Takahashi H (2013) Design, synthesis, and biological evaluations of novel 7-[7-amino-7-methyl-5-azaspiro[2.4]heptan-5-yl]-8-methoxyquinolines with potent antibacterial activity against respiratory pathogens. *J Med Chem* **56**:1974-1983.

- Pearson JT, Wahlstrom JL, Dickmann LJ, Kumar S, Halpert JR, Wienkers LC, Foti RS, and Rock DA (2007) Differential time-dependent inactivation of P450 3A4 and P450 3A5 by raloxifene: a key role for C239 in quenching reactive intermediates. *Chem Res Toxicol* **20**:1778-1786.
- Sevrioukova IF and Poulos TL (2013) Understanding the mechanism of cytochrome P450 3A4: recent advances and remaining problems. *Dalton Trans* **42**:3116-3126.
- Takakusa H, Wahlin MD, Zhao C, Hanson KL, New LS, Chan EC, and Nelson SD (2011) Metabolic intermediate complex formation of human cytochrome P450 3A4 by lapatinib. *Drug Metab Dispos* **39**:1022-1030.
- Thummel KE and Wilkinson GR (1998) In vitro and in vivo drug interactions involving human CYP3A. *Annu Rev Pharmacol Toxicol* **38**:389-430.
- Wang H, Dick R, Yin H, Licad-Coles E, Kroetz DL, Szklarz G, Harlow G, Halpert JR, and Correia MA (1998) Structure-function relationships of human liver cytochromes P450 3A: aflatoxin B1 metabolism as a probe. *Biochemistry (Mosc)* **37**:12536-12545.
- Wang YH, Jones DR, and Hall SD (2005) Differential mechanism-based inhibition of CYP3A4 and CYP3A5 by verapamil. *Drug Metab Dispos* **33**:664-671.

- Watanabe A, Nakamura K, Okudaira N, Okazaki O, and Sudo K (2007) Risk assessment for drug-drug interaction caused by metabolism-based inhibition of CYP3A using automated in vitro assay systems and its application in the early drug discovery process. *Drug Metab Dispos* **35**:1232-1238.
- Watanabe A, Takakusa H, Kimura T, Inoue S, Kusuhara H, and Ando O (2016) Analysis of Mechanism-Based Inhibition of CYP 3A4 by a Series of Fluoroquinolone Antibacterial Agents. *Drug Metab Dispos* **44**:1608-1616.
- Wilkinson GR (2005) Drug metabolism and variability among patients in drug response. *N Engl J Med* **352**:2211-2221.

Figure legends

Fig. 1. Reversibility of MBI of CYP3A5 by fluoroquinolone compounds in recombinant human CYP3A5 Supersomes. The percentage of control data after 0-minute preincubation followed by incubation with (dark gray) or without (black) potassium ferricyanide and that after 30-minute preincubation followed by incubation with (white) or without (light gray) potassium ferricyanide were obtained. Concentration of the test compounds was 100 μ M except for compounds 2 and 4, the concentration of which was 30 μ M. Each bar represents mean \pm SD of triplicate experiments. * $P < 0.01$. NS, not significant.

Fig. 2. Absorbance difference between 455 and 490 nm of CYP3A5 incubated with compound 6 (circle), 8 (square), or 10 (triangle) for 20 minute after the addition of NADPH-generating system. Each symbol represents mean \pm SD of triplicate experiments. No significant difference ($p < 0.01$) was observed between absorbance at 0 minute and each subsequent time point.

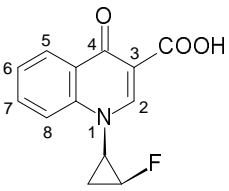
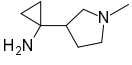
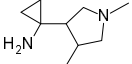
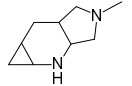
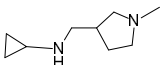
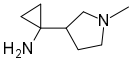
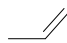
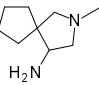
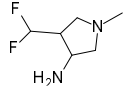
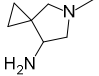
Fig. 3. Structure of compound 1 and proposed structures of metabolites generated from compound 1.

Fig. 4. Structure of compound 6 and proposed structures of metabolites generated from compound 6.

Fig. 5. (A) CYP3A5 homology model (pink) superposed with CYP3A4 X-ray structure (gray). Nine hydrophobic residues of CYP3A5 that differ from those of CYP3A4 and heme are indicated as tube model. Structure of CYP3A5 is shown as ribbon model and solvent-accessible surface in white. (B) CYP3A5 homology model was superposed using docking model of compound 6 or (C) its nitroso metabolite to CYP3A4. Binding to CYP3A5 would be affected by the pocket shape.

Fig. 6. Effect of amino acid residue at position 210 in CYP3A4 and CYP3A5 for binding the nitroso intermediate of compound 6. The molecular surface of the nitroso intermediate of compound 6 is shown in green. The molecular surfaces of different amino acid residues around the nitroso intermediate between CYP3A4 and CYP3A5 are shown in (A) yellow and (B) pink, respectively.

Table 1. Structures of fluoroquinolone compounds tested in this study. Substructures of positions C1–C5 in a quinolone scaffold are common among all compounds. Each substructure of positions C6–C8 is shown below.

Common scaffold			
	Position		
	C-6	C-7	C-8
Compound 1	—H		—O—
Compound 2	—H		—O—
Compound 3	—F		—O—
Compound 4	—F		—O—
Compound 5	—F		
Compound 6	—F		—O—
Compound 7	—F		—O—
Compound 8	—F		—O—

DMD #73783

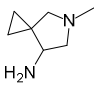
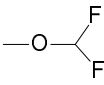
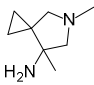
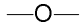
Compound 9	—F		
Compound 10	—F		

Table 2. Comparison of the inhibitory potential of fluoroquinolone compounds on CYP3A4 and CYP3A5. The % remaining data indicate the percentage of the enzymatic activity remaining after 30-minute preincubation relative to 0-minute preincubation with each compound followed by incubation without potassium ferricyanide. The data for CYP3A4 and CYP3A5 were calculated from the results of the metabolic activity obtained in our previous report (Watanabe et al., 2016) and in Figure 1 of this study, respectively. Values are shown as mean \pm standard deviation (S.D.) of triplicate experiments.

	CYP3A4		CYP3A5	
	Concentration	% remaining	Concentration	% remaining
Compound 1	100 μ M	32.1 \pm 4.4	100 μ M	41.3 \pm 1.4
Compound 2	30 μ M	46.4 \pm 1.9	30 μ M	33.9 \pm 2.4
Compound 3	100 μ M	42.4 \pm 1.8	100 μ M	70.5 \pm 2.1
Compound 4	30 μ M	45.3 \pm 2.1	30 μ M	58.0 \pm 2.8
Compound 5	30 μ M	47.0 \pm 1.5	100 μ M	44.3 \pm 2.5
Compound 6	10 μ M	46.4 \pm 1.5	100 μ M	100 \pm 4
Compound 7	100 μ M	60.1 \pm 3.0	100 μ M	101 \pm 1
Compound 8	100 μ M	62.2 \pm 2.1	100 μ M	102 \pm 1

DMD #73783

Compound 9	30 μ M	57.7 \pm 1.8	100 μ M	103 \pm 3
Compound 10	100 μ M	101 \pm 13	100 μ M	106 \pm 12

Fig. 1.

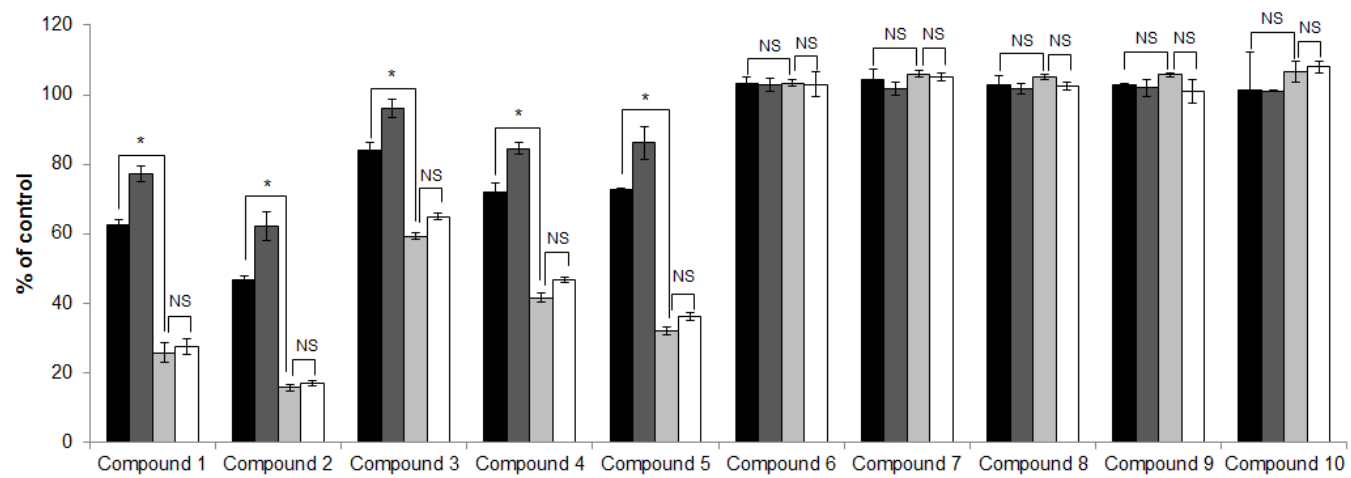


Fig. 2.

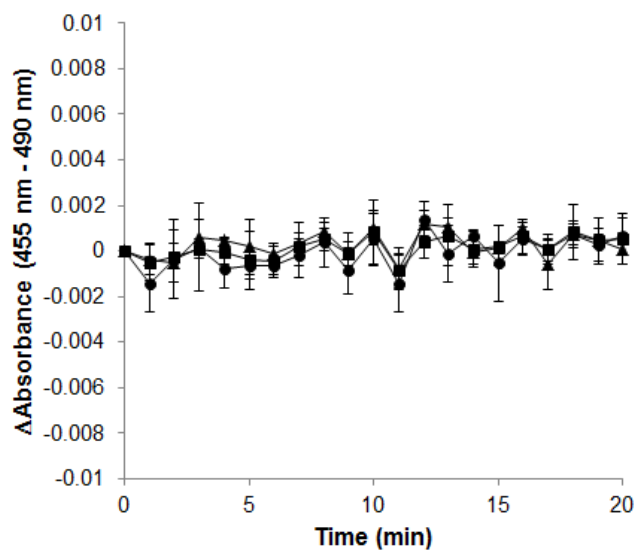


Fig. 3.

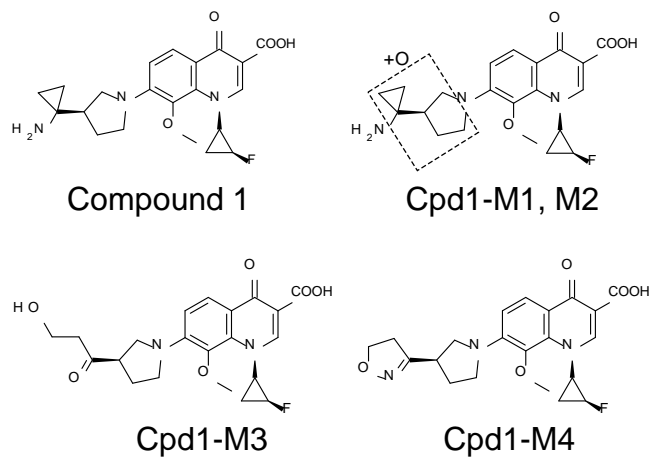
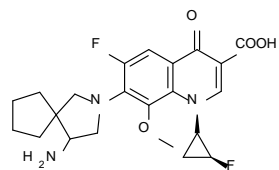
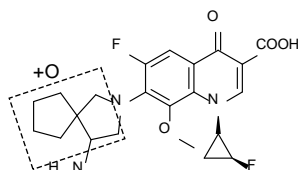


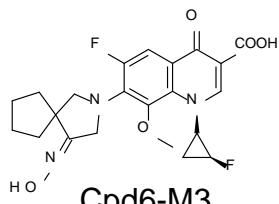
Fig. 4.



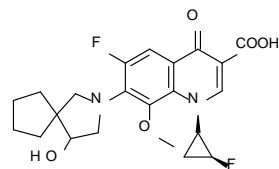
Compound 6



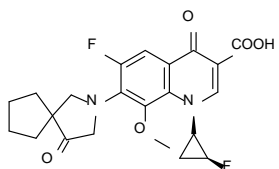
Cpd6-M1, M2



Cpd6-M3



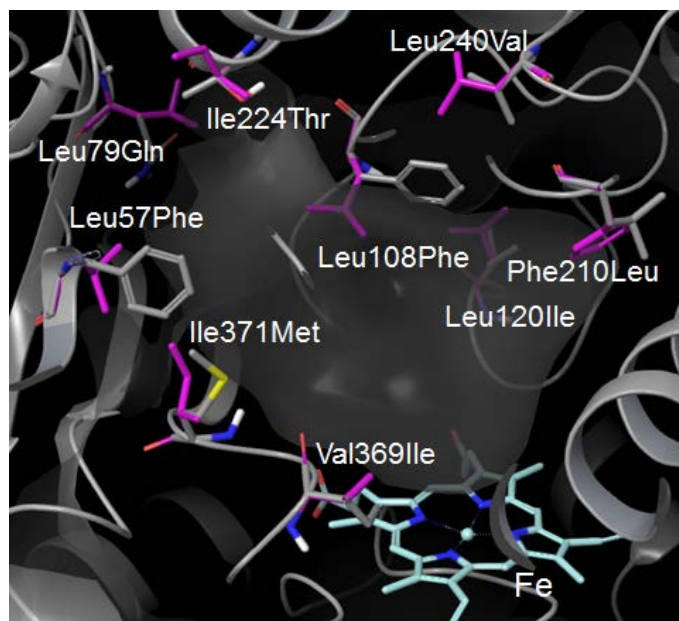
Cpd6-M4



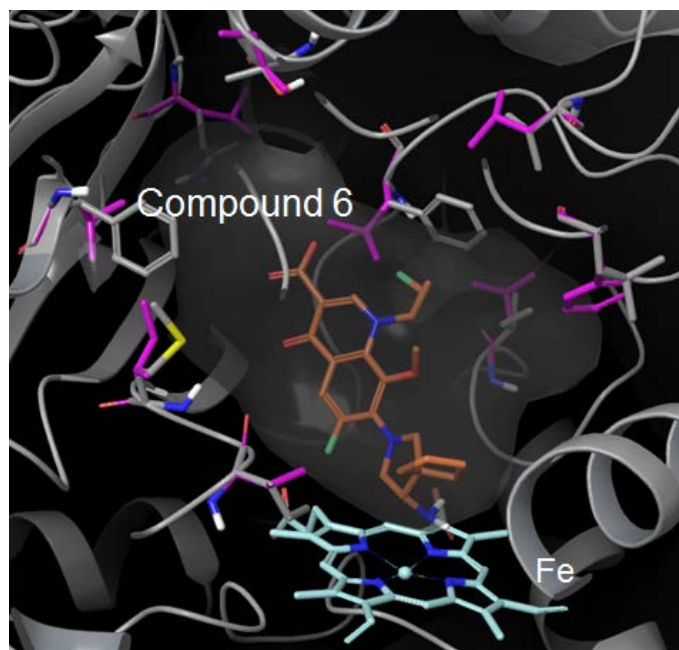
Cpd6-M5

Fig. 5.

A



B



C

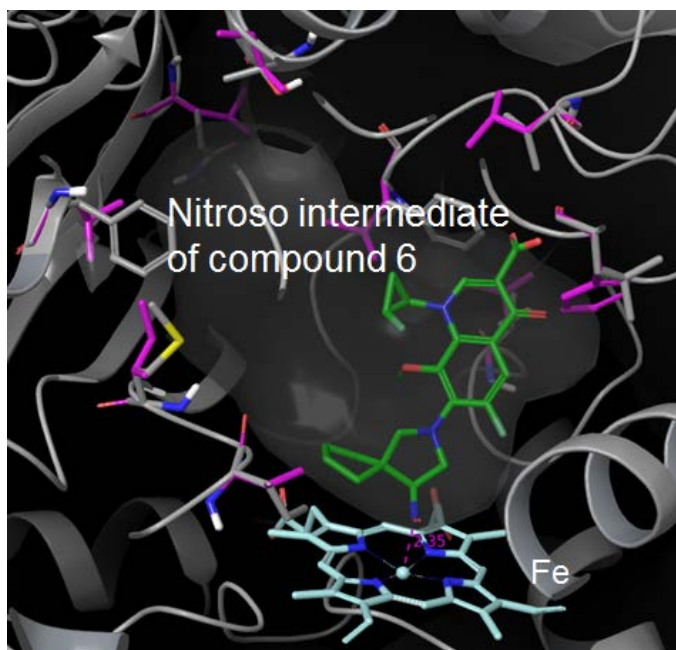
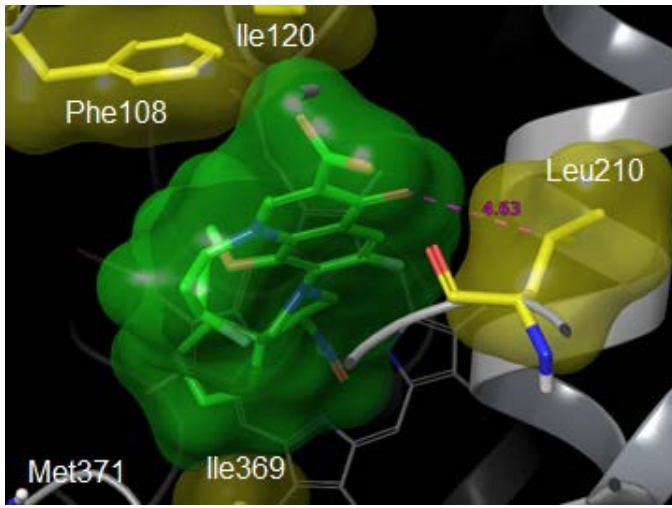


Fig. 6.

A



B

